RSC Advances

PAPER

View Article Online
View Journal | View Issue

Cite this: *RSC Adv.*, 2020, **10**, 17353

Wrist flexible heart pulse sensor integrated with a soft pump and a pneumatic balloon membrane†

Takafumi Yamaguchi,[a] Daisuke Yamamoto,[a] Takayuki Arie,[a] Seiji Akita[a] and Kuniharu Takei *[ab]

Received 12th March 2020
Accepted 24th April 2020

DOI: 10.1039/d0ra02316g

rsc.li/rsc-advances

To monitor health and diagnose disease in the early stage, future healthcare standards will likely include the continuous monitoring of various vital data. One approach to collect such information is a wearable and flexible device, which detects information from the skin surface. An important dataset is heart pulse information. Herein a method to monitor the detailed pulse signal from a wrist stably and reliably is proposed. Specifically, a soft pneumatic balloon operated by a soft pump applies the appropriate pressure over a tactile sensor onto the radial artery of the wrist to detect detailed heart pulse waves. The soft pump, pneumatic balloon, and flexible tactile pressure sensor are characterized as a fundamental study. Additionally, a proof-of-concept of this integrated device platform is demonstrated by monitoring the heart pulse from a wrist with and without the soft pump functions.

Introduction

Continuous real-time healthcare monitoring has received much attention for near-future medical and healthcare applications. For example, such monitoring can diagnose disease in the early stage, which patients often do not feel by themselves. Wearable devices should monitor real-time healthcare and conditions comfortably. However, detectable information of a wristband-type wearable device is limited due to poor contact with the skin surface. In fact, most commercial wristband-type (or watch) devices only measure activity and heart pulse using an accelerometer and optical reflection, respectively, because these methods do not require good skin contact. To increase health condition datasets available from the skin surface, bandage-type attachable flexible sensor sheets with multi-functionalities, which are in direct contact with the skin surface, have been widely studied.[1–5] Direct contact between the sensor and skin allows various vital information to be precisely measured such as skin temperature,[6] perspiration rate,[7] sweat chemical content,[8–13] heart pulse,[14–17] respiration,[18] electrocardiogram,[19–22] and activity.[23,24] Although more research is necessary to realize practical flexible sensor sheets, this platform holds promise to identify minor changes in health conditions and disease in the early stage.

One requirement for continuous monitoring is to stably and precisely measure health conditions. Recently, precise skin temperature monitoring has been realized by considering the thermal management structure.[6] Based on this development, relatively stable and precise skin temperature can be recorded in real-time regardless of environmental temperature changes. Similarly, heart pulse monitoring from the wrist is important vital data that requires precise and stable recording. Flexible tactile pressure sensors have been successfully used to observe a small pressure change from the wrist caused by the radial artery.[15,16] Furthermore, self-powered pulse sensors from the wrist have been studied by using triboelectric and piezoelectric materials.[25–27] The advantage of the self-powered sensor is to reduce power consumption for the long-time monitoring. However, for both techniques, power source is still required. More importantly, stable detection of the heart pulse even after activity remains a challenge.

In terms of heat pulse detection from a wrist, a commercially available wearable device can detect heart pulse rate using the optical reflection method. However, this can only monitor the heart pulse rate. For the precise healthcare application, more detailed signals of the pulses, consisting of 2–3 pulses in a heart pulse, from the wrist are often required to diagnose.

To realize stable and detailed heart pulse detection using a tactile pressure sensor on a wrist, this study proposes integrating a pneumatic-based soft pump and a pneumatic balloon to maintain the sensor position and proper pressure onto the skin with a flexible tactile pressure sensor. The fundamental characteristics of the pump, pneumatic balloon, and pressure sensor as well as a proof-of-concept demonstration of heart pulse detection are discussed.

Device design

The device consists of three main parts (Fig. 1a). The detailed device design is described in Fig. S1.† The first part is a soft material-based pump with a check valve. The pump is operated

[a]*Department of Physics and Electronics, Osaka Prefecture University, Sakai, Osaka 599-8531, Japan. E-mail: takei@pe.osakafu-u.ac.jp*

[b]*Japan Science and Technology, PRESTO, Kawaguchi, Saitama 332-0012, Japan*

† Electronic supplementary information (ESI) available. See DOI: 10.1039/d0ra02316g

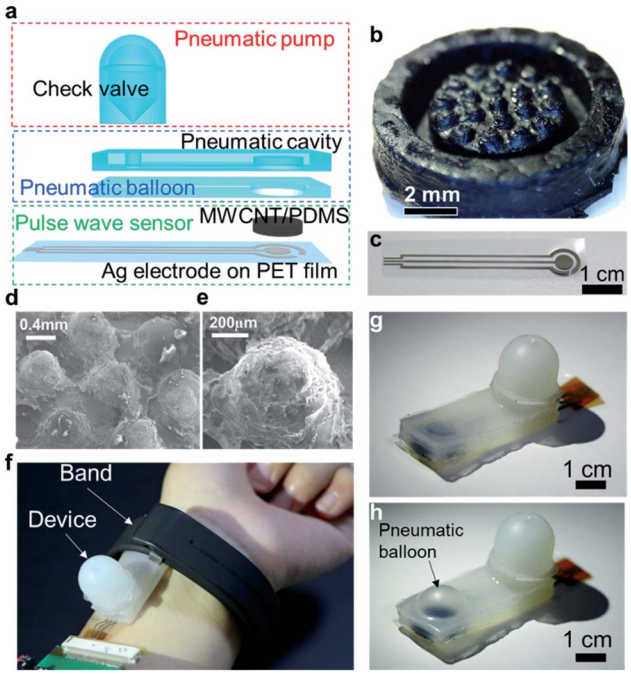

Fig. 1 (a) Schematic of the device structure. Photos of (b) the MWCNT/PDMS layer and (c) Ag electrodes on a PET film for a flexible tactile pressure sensor. SEM images of (d) the microcone structure of the MWCNT/PDMS layer and (e) magnification of the microcone structure. (f) Photo of the wearable pump and balloon-integrated flexible tactile pressure sensor fixed by a band on a wrist. Photos of the pneumatic balloon membrane (g) without and (h) with air pressure.

manually. To block the backflow of air, oil is applied in the valve region. The second part is a soft pneumatic balloon structure. The Ecoflex membrane can be inflated by applying air pressure generated by the soft pump. The last part is a tactile pressure sensor. A cone-structured conductive polydimethylsiloxane (PDMS) layer mixed with multi-walled carbon nanotubes (MWCNTs) (Fig. 1b) is used to create a contact with Ag electrode printed on a polyethylene terephthalate (PET) film (Fig. 1c). This contact area, which corresponds to the contact resistance, changes as a function of the applied tactile pressure.

The surface morphology of the MWCNT/PDMS was observed by scanning electron microscopy (SEM). Fig. 1d and e exhibit a rough surface due to the relatively high concentration of MWCNT (10 wt%) in the PDMS film. 10 wt% MWCNT in PDMS was chosen because the conductivity was poor if low concentration of MWCNT was used. The device is used by placing it between the skin at the wrist and the band (Fig. 1f). For the soft pump and pneumatic balloon, applying air pressure from the soft pump inflates the thin membrane of the balloon (Fig. 1g and h). Because this sensor is attached onto a wrist using a band similar to that of a watch, balloon membrane pushes the sensor onto the skin.

Results and discussion

Soft pump and pneumatic balloon

The soft pump is operated by squeezing the Ecoflex structure manually to push air from the check valve to the pneumatic balloon membrane (Fig. 2a and b). Due to the small hole on the top of the pump, after one squeeze, air is supplied from the outside. By repeatedly pumping, the air is pressurized and pushed to the Ecoflex membrane to create a certain height (Fig. 2b).

The height and generated force were systematically characterized as functions of the pumping cycle and usage. The height of the balloon structure linearly increases at a rate of 2.1 mm per pumping cycle as the pumping cycle increases (Fig. 2c). Importantly, the results for multiple usages in this study are consistent.

Similarly, the generated force measured depends on the pumping cycle and repeating times. To measure the force, a force gauge sensor was placed on the balloon structure. As expected, the generated force increases as the pumping times increase (Fig. 2d). This trend agrees well with the results in Fig. 2c. However, after pumping three times, the generated force is almost saturated around 1.5 N. This is because the force gauge sensor also pushes the balloon membrane and the air most likely returns to the pump through the check valve with back flow due to the increased air pressure in the channel. Since this balloon membrane is placed between the skin and the band, this situation is the real use of the sensor, suggesting that the maximum

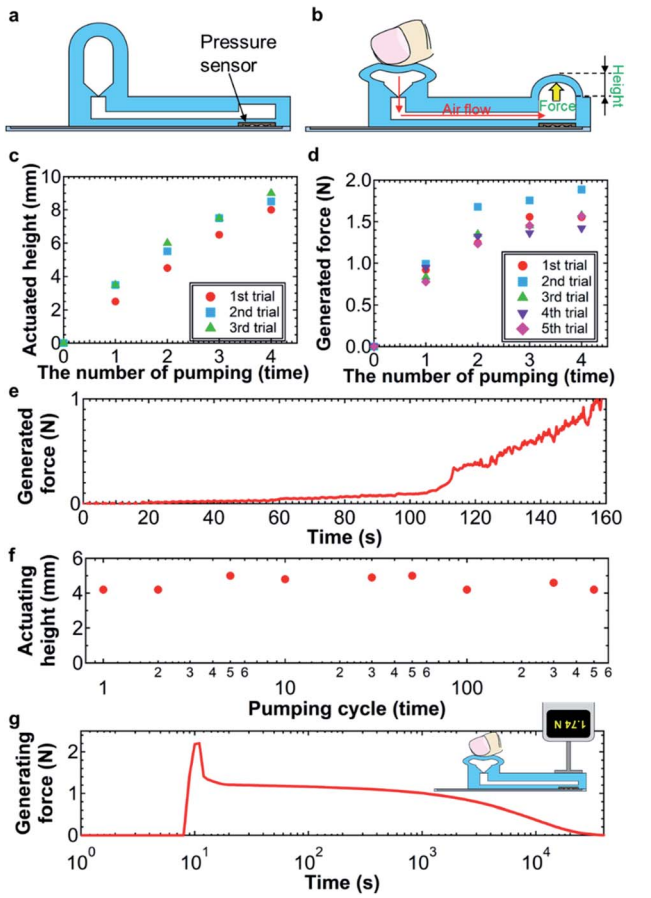

Fig. 2 Schematics (a) without and (b) with a soft pump operation by a finger. Height is defined by the deformation, as described in (b). (c) Balloon height and (d) generated force as functions of pumping time. Repeatable measurement results are shown. (e) Real-time generated force for one pump push application. (f) Pumping cycle test to observe the balloon height. (g) Retention time of the pneumatic balloon force after operating the pump.

balloon force is ~1.5 N. During one-time pumping, the generated force by the soft pump gradually increases by increasing the applied deformation of the pump (Fig. 2e), indicating that the small applied force can be controlled by integrating a pressure sensor on the sensor or pump. However, such integration is beyond the scope of this study.

Next, the mechanical robustness of the soft pump and pneumatic balloon is discussed. Sustained use of the pump and pneumatic balloon were characterized by repeating the pumping cycles. The balloon height is consistent at 4.6 ± 0.4 mm up to 500 cycles (Fig. 2f). Based on the results, the soft pump and pneumatic balloon with a check valve are mechanically robust for wearable applications.

Another important characteristic is the retention time of the applying force. Fig. 2g shows the force generated by the pneumatic balloon structure for a long-time measurement after pumping. In this experiment, the force gauge sensor was placed on the balloon membrane without any gaps. Due to this setup, after applying the pumping function, the force drops quickly from 2.2 N to 1.2 N due to back flow of air through the check valve, as discussed in Fig. 2d. After the force pressure drops, the force becomes relatively stable around 1.2 N. However, after 2 hours, the force gradually decreases and eventually reaches 0 N at 8.5 hours. For practical applications, continuous monitoring for at least one day will be required. This air pressure degradation is most likely due to leakage of air back-flow *via* the check valve. To realize a practical device platform, this instability of the air pressure generation needs to be addressed by optimizing the check valve structure and material in the future.

Tactile pressure sensor

To monitor the displacement generated by a pulse from the wrist, a highly sensitive tactile pressure sensor must be integrated with the soft pump and pneumatic balloon structure. For this purpose, a contact-based resistive tactile pressure sensor was fabricated. Fig. 3a and b describe the sensing mechanism. A sub-millimeter-scale conductive cone structure was placed over the Ag electrode-printed PET film. The resistance change between the Ag electrode and cone-structured MWCNT/PDMS was measured as a function of the applied pulse. The PET film was placed directly onto the wrist to transfer the pulse pressure. Applying a pulse pressure deforms the PET film (Fig. 3b). This deformation makes the electrical contact between MWCNT/PDMS and the Ag electrodes. The contact area corresponding to the contact resistance depends on the pulse pressure.

To confirm this behavior, the resistance was measured as a function of the applied force. Fig. 3c indicates that the resistance drastically decreases as the applied force increases until the resistance value reaches the saturation level at a high force above 0.6 N. This saturation is most likely due to the limitation of MWCNT/PDMS deformation and softness. More importantly, the hysteresis of the resistance change is almost negligible with forward and backward applied force sweeps (Fig. 3c). For pulse monitoring, the response speed should be less than 0.1 s. Fig. 3d indicates the response and recovery time is around 20 ms, which is sufficient for the pulse and other wearable device applications.

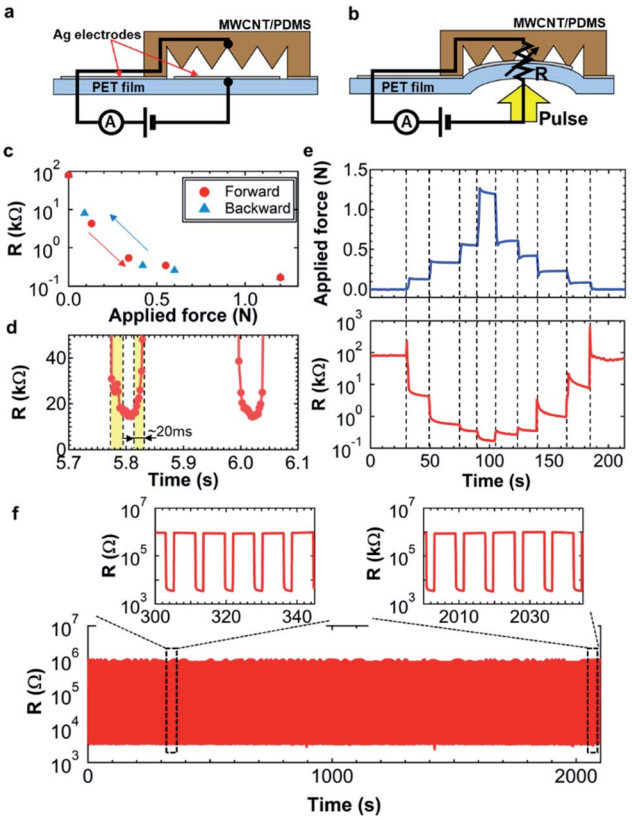

Fig. 3 Schematics (a) without and (b) with an applied force over the tactile pressure sensor. (c) Resistance change as a function of the applied force. (d) Response time measurement of the sensor. (e) Real-time continuous force monitoring. (Top) Applied force and (bottom) resistance of the sensor corresponding to the applied force. (f) Cycle test at ~0.2 N applied force for more than 1100 cycles.

After evaluating the fundamental properties of the tactile pressure sensor, continuous real-time detection and long-time reliability were tested for practical use. First, a force was continuously applied to the sensor (Fig. 3e). The resistance of the sensor changes with the applied pressure. For example, around 140 s, some spike signals are observed when the applied force is changed. These spiked signals are not artifacts or errors of the sensor. They match well with the small applied force change, suggesting that this sensor has a high sensitivity and a high reliability. Furthermore, the hysteresis is negligible (Fig. 3c).

For a wearable application, a long-time multiple cycle detection is another important factor. A ~0.2 N force was repeatedly applied on the sensor. The resistance change is constant for more than 1100 cycles (Fig. 3f). Importantly, the output behaviors are almost the same from the beginning to the end (Fig. 3f, inset). Based on the results, the tactile pressure sensor is relatively stable for measurements of heart pulse monitoring from a wrist.

Heart pulse detection

As a proof-of-concept of the soft pump-integrated flexible tactile pressure sensor, the sensor was placed on the radial artery region of the wrist. To generate the force of the sensor surface to

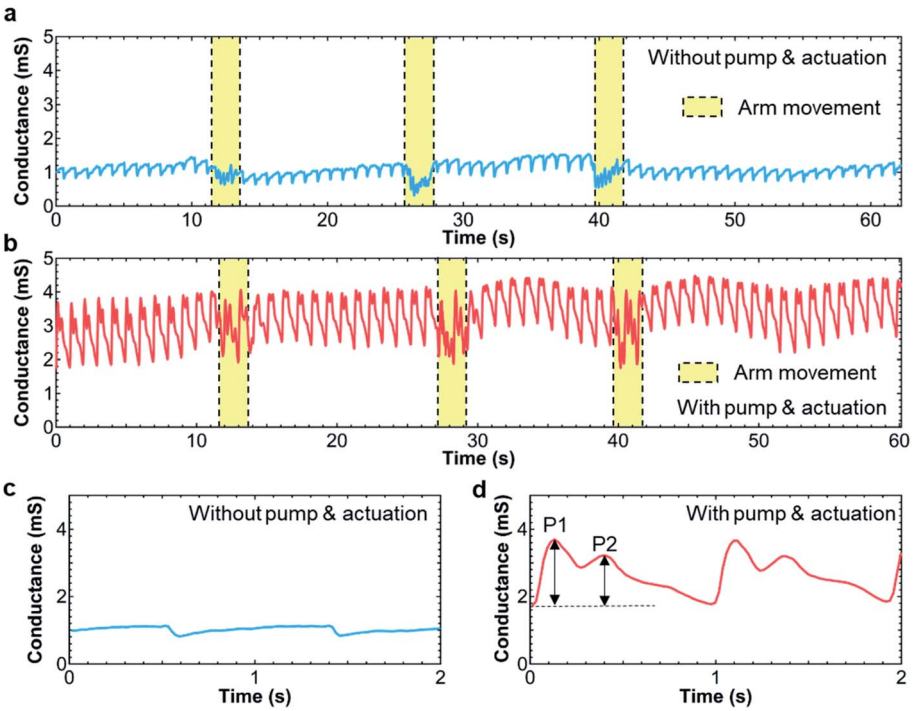

Fig. 4 Real-time heart pulse wave monitoring (a) without and (b) with pump. (c) and (d) Enlarged peaks extracted from the results of (a) and (b), respectively.

the region, the sensor system was covered by a band as shown in Fig. 1f. Before using a pump, the sensor was placed onto the skin. Due to the weak contact between the sensor and skin, the heart pulse amplitude is small (Fig. 4a). Upon applying the pump and pneumatic balloon functionalities, the output signal amplitude is enhanced more than 6 times (2 mS with the pump

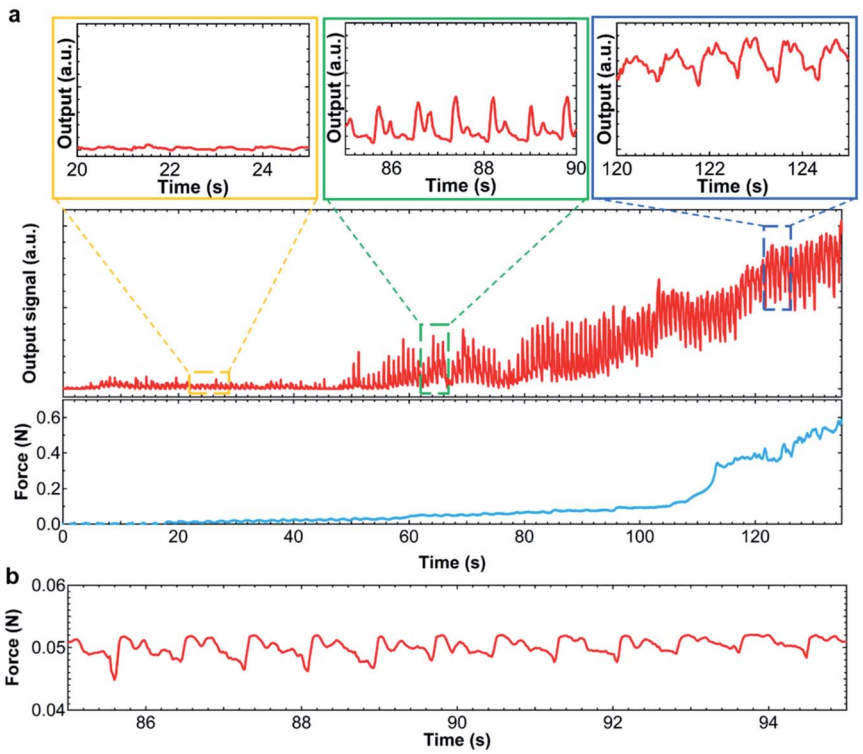

Fig. 5 (a) Heart pulse wave monitoring during one push deformation of the pump. Enlarged results for each time are also shown. Corresponding applied force to the output signal of the resistance change is also shown. (b) Real-time force to obtain the ideal heart pulse wave with two peaks. The increase of the output signal as a function of time is due to increase of the contact pressure of the sensor onto the wrist.

and 0.3 mS without the pump, Fig. 4b). To observe the pulses, conductance is used instead of the resistance because the waveform peaks (P1 and P2) of the wrist pulse in general shows the positive amplitudes. It is fair to note that the amplitude of the pulse can also be controlled by the band size. For the purpose of pump and pneumatic balloon integration without measuring and adjusting the band size, ideal heart pulse waves can be measured using the pump and balloon functionalities. Interestingly, even after wrist movement, the output signal with and without a pump function does not change, but the output signals change during movements. This stability, especially for that without a pump function, is explained by the fact that the sensor is well attached onto the wrist and the sensor does not move even under movement. Fig. 4c and d indicate that enlarged pulse signals are extracted from Fig. 4a and b, respectively. While the signal without a pump function has a peak at each pulse, the one with a pump function displays two peaks, which correspond to P1 and P2 pulse waves. (See ESI Movies.†) For a detailed study on the pulses, the amplitudes of both the P1 and P2 peaks are important. Based on these demonstration results, the pump and balloon functionalities can control the applied pressure between the sensor and skin, allowing detailed peaks from the radial artery region to be analyzed.

To shed further light on the pneumatic balloon pressure dependence for pulse detection, the force dependence in terms of the pulse wave shape is analyzed. By gradually applying air pressure, the amplitude of the pulse wave increases (Fig. 5a). At a low air pressure, as discussed in Fig. 4c, the amplitude is too small to read the detailed peaks of P1 and P2. For detailed pulse wave detection, the ideal applied force was extracted from the results in Fig. 5a. These two peaks can be clearly observed at a pressure of ~30–70 mN (Fig. 5b). It should be noted that only one peak with a small split can be monitored (Fig. 5a), when further air pressure is applied due to the low sensitivity of the sensor at a higher air pressure, confirming that air pressure control is important to monitor a heart pulse from the wrist precisely and stably.

Conclusion

This study demonstrates the integration of a soft pump and a pneumatic balloon with a flexible tactile pressure sensor to detect detailed pulse waves (P1 and P2) from the radial artery region of the wrist. By optimizing the device structure, including the pump, balloon, and sensor, detail peaks of P1 and P2 can be clearly monitored after using the pump. Furthermore, the ideal air pressure to monitor pulse waveforms is discussed based on the experimental results. This sensor system has the potential to monitor stable pulse waves from the wrist as a wearable device. To realize practical wearable device applications, other developments are required such as wireless/signal processing integration, signal analysis systems, and real-time long-time pulse wave detection in the future. In addition, soft pump and valve need to be much smaller for the wearable application by optimizing the device design. Although a lot of challenges are still remained, there are some potential applications such as blood pressure estimation if stable heart pulse detection is realized. This real-time, wearable multi vital information monitoring may change the healthcare and medical methods.

Experimental

Device fabrication process

Fig. S2† overviews the fabrication process. First, MWCNT (#724769, Aldrich) and a PDMS composite solution (Sylgard 184, Dow Corning) were mixed at a 1 : 9 wt% ratio. The solution was poured into a 3D printed mold with microcone structures (1 mm high and 1 mm diameter) (Fig. S2a(1)†). After curing the solution at 90 °C for more than 2 hours (Fig. S2a(2)†), the MWCNT/PDMS film with a cone structure was delaminated from the mold (Fig. S2a(3)†). In parallel, Ag electrodes were screen-printed on a 12 μm-thick PET film and cured at 90 °C for 1 hour (Fig. S2a(4)†). Then the MWCNT/PDMS film was laminated using Ag electrode ink (Fig. S2a(5)†). Next, the soft pump, check valve, and pneumatic balloon membrane were fabricated using soft lithography and 3D printing (Fig. S2b(1)†). Afterwards, an Ecoflex solution (Ecoflex 0030, Smooth-On) was poured into the molds and cured at 90 °C for 2 hours (Fig. S2b(2)†). After delamination of the Ecoflex-based structures from the molds (Fig. S2b(3)†), lubricant oil was applied at the tip of the valve to prevent air back flow through the check valve. All Ecoflex components were then bonded using the Ecoflex solution as a glue at 90 °C for 1 hour (Fig. S2a(4)†). Finally, a tactile pressure sensor consisting of the MWCNT/PDMS/PET film was laminated under the Ecoflex structures. The Ecoflex solution was again used to bond these structures at the same condition (Fig. S2c†).

Characterization

Electrical responses of the tactile pressure sensor were measured using a semiconductor analyzer (B1500A, Keysight) for precise characteristics. The long-time monitoring of cycles test and heart pulse detection was performed using a memory data logger (LR8401, Hioki) and a high speed high data logger (MR6000, Hioki), respectively. The force measurements to characterize the tactile pressure sensor and soft pump were conducted by using a force measurement system (ZTS Series, IMADA).

Heart pulse monitoring

The tactile pressure sensor devices were placed between the wrists of two volunteers and a band. It was connected to the data logger to monitor the heart pulse waves. The experiments were performed in compliance with a protocol approved by Osaka Prefecture University. Informed consent was received from the volunteers.

Conflicts of interest

The authors declare no competing financial interest.

Acknowledgements

This work was supported by JST PRESTO (JPMJPR17J5) and JSPS KAKEN Grants (JP17H04926 & JP18H05472).

References

1 Y. H. Jung, B. Park, J. U. Kim and T. I. Kim, *Adv. Mater.*, 2019, **31**, e1803637.
2 Y. Liu, M. Pharr and G. A. Salvatore, *ACS Nano*, 2017, **11**, 9614–9635.
3 D. H. Kim, N. Lu, R. Ma, Y. S. Kim, R. H. Kim, S. Wang, J. Wu, S. M. Won, H. Tao, A. Islam, K. J. Yu, T. I. Kim, R. Chowdhury, M. Ying, L. Xu, M. Li, H. J. Chung, H. Keum, M. McCormick, P. Liu, Y. W. Zhang, F. G. Omenetto, Y. Huang, T. Coleman and J. A. Rogers, *Science*, 2011, **333**, 838–843.
4 K. Takei, W. Honda, S. Harada, T. Arie and S. Akita, *Adv. Healthcare Mater.*, 2015, **4**, 487–500.
5 K. Xu, Y. Lu and K. Takei, *Adv. Mater. Technol.*, 2019, **4**, 1800628.
6 K. Xu, Y. Lu, T. Yamaguchi, T. Arie, S. Akita and K. Takei, *ACS Nano*, 2019, **13**, 14348–14356.
7 Z. Yuan, L. Hou, M. Bariya, H. Y. Y. Nyein, L. C. Tai, W. Ji, L. Li and A. Javey, *Lab Chip*, 2019, **19**, 3179–3189.
8 W. Gao, S. Emaminejad, H. Y. Nyein, S. Challa, K. Chen, A. Peck, H. M. Fahad, H. Ota, H. Shiraki, D. Kiriya, D. H. Lien, G. A. Brooks, R. W. Davis and A. Javey, *Nature*, 2016, **529**, 509–514.
9 H. Lee, C. Song, Y. S. Hong, M. S. Kim, H. R. Cho, T. Kang, K. Shin, S. H. Choi, T. Hyeon and D.-H. Kim, *Sci. Adv.*, 2017, **3**, e1601314.
10 S. Nakata, T. Arie, S. Akita and K. Takei, *ACS Sens.*, 2017, **2**, 443–448.
11 S. Nakata, M. Shiomi, Y. Fujita, T. Arie, S. Akita and K. Takei, *Nat. Electron.*, 2018, **1**, 596–603.
12 A. J. Bandodkar, P. Gutruf, J. Choi, K. Lee, Y. Sekine, J. T. Reeder, W. J. Jeang, A. J. Aranyosi, S. P. Lee, J. B. Model, R. Ghaffari, C.-J. Su, J. P. Leshock, T. Ray, A. Verrillo, K. Thomas, V. Krishnamurthi, S. Han, J. Kim, S. Krishnan, T. Hang and J. A. Rogers, *Sci. Adv.*, 2019, **5**, eaav3294.
13 Y. Yang, Y. Song, X. Bo, J. Min, O. S. Pak, L. Zhu, M. Wang, J. Tu, A. Kogan, H. Zhang, T. K. Hsiai, Z. Li and W. Gao, *Nat. Biotechnol.*, 2020, **38**, 217–224.
14 H. Lee, E. Kim, Y. Lee, H. Kim, J. Lee, M. Kim, H.-J. Yoo and S. Yoo, *Sci. Adv.*, 2018, **4**, eaas9530.
15 J. Park, M. Kim, Y. Lee, H. S. Lee and H. Ko, *Sci. Adv.*, 2015, **1**, e1500661.
16 Y. Gao, C. Yan, H. Huang, T. Yang, G. Tian, D. Xiong, N. Chen, X. Chu, S. Zhong, W. Deng, Y. Fang and W. Yang, *Adv. Funct. Mater.*, 2020, **30**, 1909603.
17 C. Yan, W. Deng, L. Jin, T. Yang, Z. Wang, X. Chu, H. Su, J. Chen and W. Yang, *ACS Appl. Mater. Interfaces*, 2018, **10**, 41070–41075.
18 K. Xu, Y. Lu, S. Honda, T. Arie, S. Akita and K. Takei, *J. Mater. Chem. C*, 2019, **7**, 9609–9617.
19 T. Kim, J. Park, J. Sohn, D. Cho and S. Jeon, *ACS Nano*, 2016, **10**, 4770–4778.
20 S. Imani, A. J. Bandodkar, A. M. Mohan, R. Kumar, S. Yu, J. Wang and P. P. Mercier, *Nat. Commun.*, 2016, **7**, 11650.
21 Y. Yamamoto, D. Yamamoto, M. Takada, H. Naito, T. Arie, S. Akita and K. Takei, *Adv. Healthcare Mater.*, 2017, **6**, 1700495.
22 M. Sugiyama, T. Uemura, M. Kondo, M. Akiyama, N. Namba, S. Yoshimoto, Y. Noda, T. Araki and T. Sekitani, *Nat. Electron.*, 2019, **2**, 351–360.
23 T. Yamada, Y. Hayamizu, Y. Yamamoto, Y. Yomogida, A. Izadi-Najafabadi, D. N. Futaba and K. Hata, *Nat. Nanotechnol.*, 2011, **6**, 296–301.
24 Y. Yamamoto, S. Harada, D. Yamamoto, W. Honda, T. Arie, S. Akita and K. Takei, *Sci. Adv.*, 2016, **2**, e1601473.
25 H. Ouyang, J. Tian, G. Sun, Y. Zou, Z. Liu, H. Li, L. Zhao, B. Shi, Y. Fan, Y. Fan, Z. L. Wang and Z. Li, *Adv. Mater.*, 2017, **29**, 1703456.
26 D. Y. Park, D. J. Joe, D. H. Kim, H. Park, J. H. Han, C. K. Jeong, H. Park, J. G. Park, B. Joung and K. J. Lee, *Adv. Mater.*, 2017, **29**, 1702308.
27 L. Zhao, H. Li, J. Meng and Z. Li, *InfoMat*, 2019, **2**, 212–234.

